Microstructure and Its Formation Mechanism in the Interface of Ti/NiCr Explosive Cladding Bar

Bingfeng Wang, Xiaozhou Luo, Bin Wang, Shiteng Zhao & Fangyu Xie

Journal of Materials Engineering and Performance

ISSN 1059-9495

J. of Materi Eng and Perform
DOI 10.1007/s11665-014-1321-0

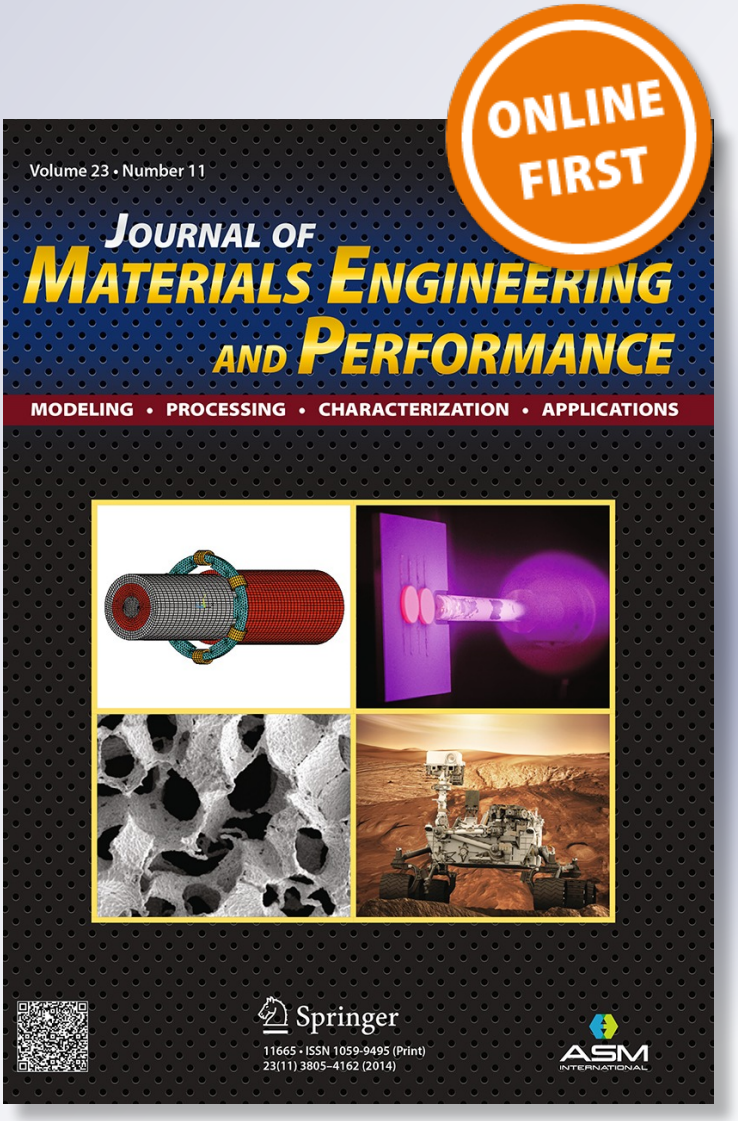

Springer

Your article is protected by copyright and all rights are held exclusively by ASM International. This e-offprint is for personal use only and shall not be self-archived in electronic repositories. If you wish to self-archive your article, please use the accepted manuscript version for posting on your own website. You may further deposit the accepted manuscript version in any repository, provided it is only made publicly available 12 months after official publication or later and provided acknowledgement is given to the original source of publication and a link is inserted to the published article on Springer's website. The link must be accompanied by the following text: "The final publication is available at link.springer.com".

Author's personal copy

JMEPEG
DOI: 10.1007/s11665-014-1321-0

©ASM International
1059-9495/$19.00

Microstructure and Its Formation Mechanism in the Interface of Ti/NiCr Explosive Cladding Bar

Bingfeng Wang, Xiaozhou Luo, Bin Wang, Shiteng Zhao, and Fangyu Xie

(Submitted September 12, 2014; in revised form November 5, 2014)

Formation of the melting zone and the heat affected zone in the Ti/NiCr cladding interface determine the quality of bonding. The microstructures and mechanical properties of the melting zone and the heat affected zone in the interface of the Ti/NiCr explosive cladding bar are investigated by means of light microscopy, electron backscattered diffraction, and transmission electron microscopy/high-resolution transmission electron microscopy. The average bonding strength of the bar is 154.39 MPa. Intermetallics, nanograins, and amorphous phases coexist in the melting zone. The heat affected zone is characterized by low hardness, low dislocation density, bulky grains, and relatively scattered grains orientation distribution. Formation mechanisms of the melting zone and the heat affected zone are described.

Keywords composites, electron backscattered diffraction, explosive cladding, grain growth, interfaces

1. Introduction

Explosive cladding is a high-strain-rate material processing method characterized by high velocity, high pressure, and high temperature (Ref 1). It is best known for its capability to join a wide variety of both similar and dissimilar combinations of metals that cannot be joined by fusion welding or any other bonding methods (Ref 2-4). In recent years, it has been increasingly employed to produce composite materials, such as Ti/steel (Ref 5, 6), AA7072/AA8090 (Ref 7), Al/Cu (Ref 8, 9), and Incoloy800/SS304 (Ref 10). Pure Ti has good biocompatibility and can be used as a body implants material. Nickel Chromium (NiCr) alloy has excellent properties such as high resistance and high strength and is often used as resistance material. If Ti tube and NiCr alloy bar were cladded together, it would be able to meet the requirements of biomedical materials such as biological compatibility and thermal properties. However, Ti and NiCr alloy has different thermal conductivity, thermal expansion coefficient, and mechanical features. Thus, explosive cladding technique is chosen to prepare Ti/NiCr alloy cladding bar.

Bingfeng Wang, School of Materials Science and Engineering, Central South University, Changsha, Hunan, People's Republic of China; Departments of Mechanical and Aerospace Engineering and Nanoengineering, University of California, SanDiego, 9500 Gilman Drive, La Jolla, CA 92093; and Key Lab of Nonferrous Materials, Ministry of Education, Central South University, Changsha, Hunan, People's Republic of China; **Xiaozhou Luo** and **Fangyu Xie**, School of Materials Science and Engineering, Centra South University, Changsha, Hunan, People's Republic of China; and **Bin Wang** and **Shiteng Zhao**, Departments of Mechanical and Aerospace Engineering and Nanoengineering, University of California, San Diego, 9500 Gilman Drive, La Jolla, CA 92093. Contact e-mail: biw009@ucsd.edu.

Local melting zones, which seriously affect the properties of the explosive cladding composite, are often encountered in sections of the cladding interface. The melting zones showed unique and interesting microstructure and properties become the hot topic of the explosive cladding technique in recent years. Yang and Wang (Ref 11) described the structural changes in the melting zones as the vortex structure during explosive cladding of titanium to titanium. The vortex zones composed of amorphous and nanograins are easy to fracture during deformation. Honarpisheh and Asemabadi (Ref 12) investigated the formation of brittle intermetallic compounds in the melting zones. The intermetallic compounds exhaust the ductility and increase the risk of brittle fracture of the deformed metal. Bamboo-shaped cracks can also be found in the melting zones (Ref 13-16). They have a negative impact on formability during the next materials processing such as rolling and extruding. Titanium and nickel are active elements. Many intermetallic compounds can be formed with titanium element and nickel element such as NiTi, $NiTi_2$, and Ni_3Ti (Ref 17). Therefore, studies on the microstructure including intermetallic compounds, nanograins, and amorphous phases in the melting zones are vital to understand the formation of the melting zones, to acquire the cladding process of the Ti/NiCr explosive cladding bar, and to formulate the next heat treatment.

The heat affected zone near the melting zone is another important part encountered in the cladding interface. Extensive researches on the heat affected zone in the explosive cladding interface have been concentrated on adiabatic shear bands. They are considered as narrow bands of intense plastic shear strain embedded in a homogeneously deformed region. The formation of adiabatic shear bands has been investigated by many researchers (Ref 18-21). Yang and Wang (Ref 6) suggested that there were two types of shear bands on the Ti side in the Ti/mild steel explosive cladding interface, and type I bands were developed from the interface and penetrated into the Ti matrix with approximate 45° inclination to the interface plane, and type II bands were formed along the wavy interface. The microstructure of shear bands on the Ti side consists of fine equiaxed grains with diameters 0.03-0.5 μm, which is regarded as the result of dynamic recrystallization (Ref 6, 18). However,

Published online: 21 November 2014

Author's personal copy

Table 1 The chemical composition and properties of the materials

Elements, wt.%	C	Si	N	S	Ti	Cr	Fe	Ni
NiCr	0.08	1.38	…	0.12	…	21.27	0.37	76.78
CP-Ti	0.08	0.02	0.03	…	99.57	…	0.30	…

	Thermal conductivity, kJ/(m * K * h)	Thermal expansion coefficient at 20 °C, 10^{-6}/K	Density, g/cm^3	Tensile strength, MPa	Modulus of elasticity, GPa	Poisson's ratio
NiCr	60.3	18	8.4	850	185	0.30
CP-Ti	58.7	8.6	4.51	344	105	0.37

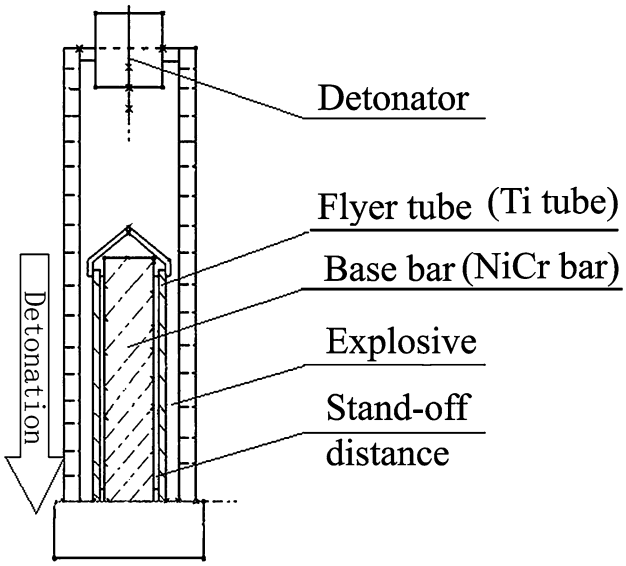

Fig. 1 Schematic view of explosive cladding process

there are few reports about the formation of the heat affected zone, especially the grain growth in it.

The aims of this paper are (1) to investigate the microstructure and mechanical properties of the melting zone and the heat affected zone in the interface of the Ti/NiCr explosive cladding bar and (2) to discuss the formation of the melting zone and the heat affected zone in the interface.

2. Experimental Procedure

The chemical composition and properties of the Pure Ti and NiCr alloy used in the present work are given in Table 1. Commercial purity titanium (CP-Ti) tube with the dimensions Φ 21 × 2 × 100 mm was used as the clad material, and NiCr alloy bar with the dimensions Φ 17 × 100 mm was used as the base material. The surfaces of the base and clad materials were used as received. The emulsified explosive with the detonation velocity 3500-4000 m/s and the density 0.8-1.0 g/cm^3 was chosen as explosive material (Ref 22). The cylindrical arrangement was used for experimental set-up for explosive cladding as schematically shown in Fig. 1. The explosive was uniformly placed around the tube. The detonator was detonated in the center of the top cap.

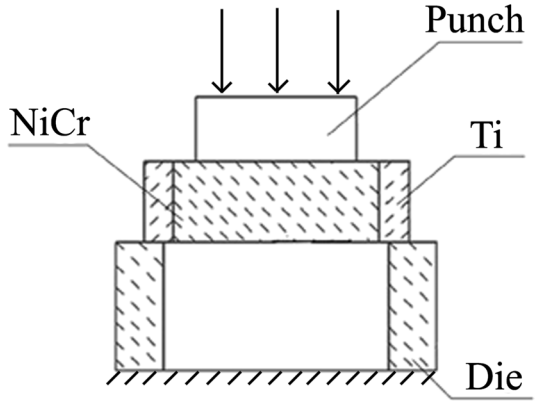

Fig. 2 Schematic of the apparatus for compression-shear experiment

We chose the classical push-out testing to investigate the shear strengths of the joint interface (Ref. 23). A universal testing machine (Instron 3369) was used to conduct the compression-shear tests (Fig. 2). The tested specimens with thicknesses of 5 mm were put on a supporting platform, with a centered circular hole of 18 mm diameter. The NiCr insert was pushed by a steel cylinder stub punch, which is concentric with the circular hole, with a diameter of 17 mm. The displacement rate of cross-head was 0.5 mm/min. Shear strength of the interface (τ) was calculated using the following equation:

$$\tau = \frac{F_{\max}}{\pi \cdot D \cdot h}, \quad \text{(Eq 1)}$$

where $F_{\max}$ is the maximum load, D is the diameter of NiCr insert, and h is the specimen thickness.

Samples for microscope observations were cut in the cross-section of the cladding bar and normal to the plane of the cladding interface. The etchant for Ti side is 4 ml HNO_3 + 6 mL HCl + 5 mL HF + 100 mL H_2O, and the NiCr alloy side is not etched. Investigations of light microscopy were performed with POLYVAR-MET. After hand grinding, the sample was reduced to a thickness of about 0.06 mm, and then the foils were perforated by electropolishing in solution of 3300 mL CH_3OH + 175 mL $C_4H_{10}O$ + 30 mL $HClO_4$ at 243 K. The transmission electron microscopy (TEM) observations were carried out with a Tecnai G^2 F20 transmission electron microscope operated at 200 kV. Electron backscattered diffraction (EBSD) measurement was carried out with a FEI Sirion 200 scanning electron microscope integrated with a computer aided EBSD system from TSL-OIM operating at

Author's personal copy

20 kV. For convenience, two sections of $\varphi_2 = 0°$, 30° in the orientation distribution function were used to illustrate texture components. All samples for analysis in this paper are cut directly from the cladding bar without homogenization heat treatment.

3. Results and Discussion

3.1 Mechanical Properties and Microstructures of the Cladding Bar's Interface

The compression-shear experiment is an important way of measuring bonding shear strength of explosive cladding bar. The mechanical results show that the bonding shear strengths of explosive cladding bar in three different sections are 152.68, 150.56, and 159.92 MPa, respectively. Thus, the average bonding shear strength of Ti/NiCr explosive cladding bar is 154.39 MPa, and it has a good bonding strength.

Figure 3 shows optical micrographs of a Ti/NiCr explosive cladding interface. It can be seen that the average thickness of the melting zone is about 80 μm with standard deviation about 138 (Fig. 3a). "A" marks the interface between the melting zone (left) and heat effected CP-Ti (right). "B" is the edge of the heat effected CP-Ti, to the right of B is unaffected Ti. The shape of the interfaces is irregular wavy curves (Fig. 3b). The heat affected zone is distinguished from the other part of the CP-Ti tube. Lots of bamboo-shaped cracks generate in the melting zone, and a few of cracks extend along the interface. They are always limited to the melting zone and do not show any tendency for crossing the cladding materials, either in the Ti tube or in the NiCr alloy bar. The sizes of grains in the heat affected zone are much larger than those in the other part of CP-Ti tube (Fig. 3c). The average grain sizes in the heat affected zone and the metal near the heat affected zone are about 60 and 4 μm, respectively (Fig. 3d).

Figure 4 shows lots of scattered solid particles in the melting zone. Some of them are the transparent snowflake nanograins with diameter about 0.1 μm (Fig. 4b). The others are big solid particles with diameters about 0.4 μm (Fig. 4c). Each solid particles has a nano-sized core. And the corresponding diffraction pattern (Fig. 4d) can be indexed as a cubic structure of NiCr.

Figure 5 shows crystal lattice image of selected area within the melting zone corresponding to Fig. 4(a). The marked "III" region is a lattice image of NiCr grains, and the marked "I" region in the left side appears as the chaos of the atomic arrangement. Therefore, the nanograins and the amorphous phases coexist in the melting zone.

3.2 Microtexture Measurement in the Interface

The EBSD technique is employed to measure the local orientations of grains within the heat affected zone and in its adjacent region in CP-Ti tube. From the measured data, the orientation distribution functions are calculated and shown in Fig. 6 and 7. The φ1, φ, and φ2 angles are the conventional Euler angles.

Figure 6 shows the grains in the region near the heat affected zone. The black points in the orientation image quality map may be caused by the emergence of high dislocations density or of a very fine microstructure which is at a smaller scale than the resolution limit of EBSD. It can be seen that the microtextures of grains in this region are peaked at (40°, 60°, 0°) and (29°, 103°, 30°) (Fig. 6b). However, the orientation distribution in the heat affected zone is relatively scattered (Fig. 7b), with some new grain orientations peak at (85°, 50°, 0°) and (60°, 70°, 30°). The average image quality values of the heat affected zone and the other region are 1504 and 1239, respectively. According to TSL software, the image quality describes the quality of Kikuchi patterns (Ref 24, 25). The image quality index can qualitatively reflect the defect density and/or lattice strain. Dislocation density causes the change of the image quality index of the EBSD measured. Therefore, the bulky grains with low dislocation density and new orientation distribution are formed in the heat affected zone.

3.3 Microstructural Formation of the Melting Zone

The melting zone plays a crucial role in deciding the quality of bonding. It is important to identify the microstructure of the zone and discuss its related formation mechanism. In this work, the average thickness of the melting zone is about 80 μm. The intermetallics TiNi and $Ti_{0.98}Ni_{1.02}$ (Ref 22), nanograins NiCr, and amorphous phases are found in the melting zone. They are often considered as the result of the extreme rapid solidification. The high cooling rates and the high pressure lead to the "creation" of crystalline intermetallic phases (Ref 7). However, formation of amorphous phases not only depends on a fast cooling rate at the beginning, but also requires the cooling rate reaching a certain degree at the amorphous transition temperature (Ref 26). Thus, the study on the formation of amorphous phases in the melting zone should build the temperature model of the melting zone firstly.

The temperature field of the explosive cladding interface can be illustrated as follows (Ref 22, 26):

$$T(0,t) = T_{\mathrm{m}} \cdot \sqrt{\frac{t_{\mathrm{r}}}{t}} \quad (t \succ t_{\mathrm{r}}), \tag{Eq 2}$$

$$\frac{\partial T}{\partial t} = -\frac{T_{\mathrm{m}}}{2} \cdot \sqrt{t_{\mathrm{r}}} \cdot \frac{1}{\sqrt{t^3}} \quad (t \succ t_{\mathrm{r}}), \tag{Eq 3}$$

where t_{r} is the time of detonation wave back to explosive cladding interface, and T, T_{m}, and t are the temperature, the melting point, and time, respectively. The parameter t_{r} is defined as follows:

$$t_{\mathrm{r}} = \frac{2H}{C_0}, \tag{Eq 4}$$

where H is the thickness of clad material and C_0 is the speed of volume wave. The physical parameters of the Ti/NiCr explosive cladding bar are as follows: the parameters H, T_{m}, and C_0 are 2 mm, 1941 K (1668 °C), and 4695 m/s, respectively. Then, the t_{r} is 0.852 microseconds (μs), and the solidification rate is shown as follow:

$$T(0,t) = 1.792 \cdot t^{-\frac{1}{2}}, \quad (t \succ 0.852\,\mu\mathrm{s}) \tag{Eq 5}$$

$$\frac{\partial T}{\partial t} = -0.896 \cdot t^{-\frac{3}{2}}. \tag{Eq 6}$$

Our previous work (Ref 11) suggested that the amorphous transition temperature of Ti ranged from 485 K (212 °C) to 630 K (357 °C). Substituting Eq 6 into Eq 5, the relation between the cooling rate (V) and temperature can be obtained (Fig. 8). It can be seen that the cooling rates (V) are 1.78×10^7 K/s (1.78×10^7 °C/s) and 3.89×10^7 K/s (3.89×10^7 °C/s) at the

Author's personal copy

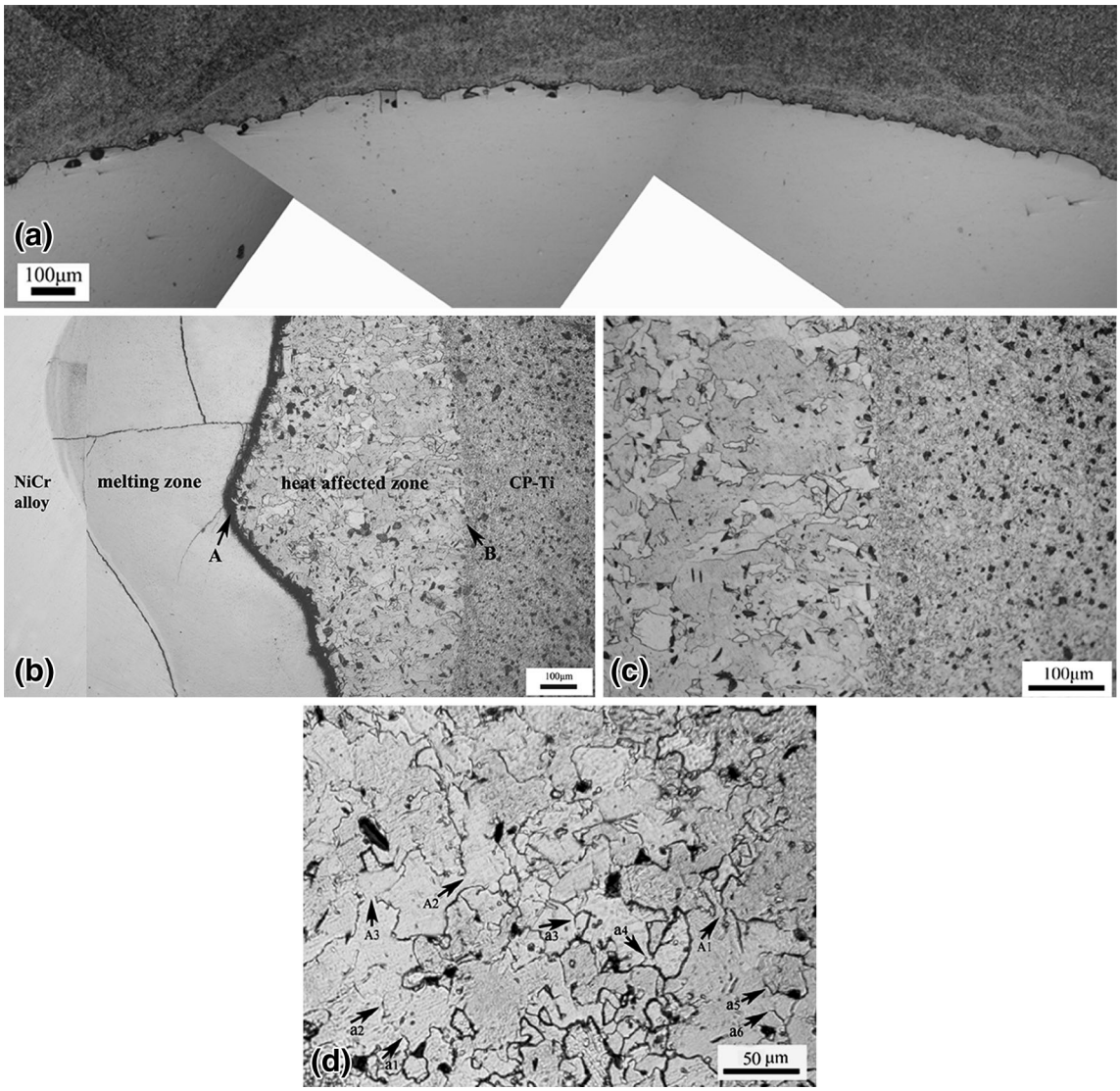

Fig. 3 Optical micrographs of explosive cladding bar's interface, (a) montage of the interface of Ti/NiCr explosive cladding bar (cross section), (b) microstructure in the cladding interface, (c) the boundary of the heat affected zone, and (d) microstructure in the heat affected zone. "A" marks the interface between the melting zone (left) and heat effected CP-Ti (right). "B" is the edge of the heat effected CP-Ti, to the right of B is unaffected Ti. Grain boundaries are marked by symbols "a1", "A1", "a2", "A2", "a3", etc.

temperature 485 K (212 °C) and 630 K (357 °C), respectively. They are larger than the usual requirement of cooling rate 1.00×10^5 K/s (1.00×10^5 °C/s) for the formation of amorphous phases. Therefore, this condition is in favor of the formation of amorphous phases. In the region slightly away from the interface, the cooling rate is not enough to form the amorphous phases and then the nanograins are formed. Therefore, the amorphous phases and nanograins coexist in the melting zone.

According to our previous works (Ref 22), two kinds of the intermetallic compounds TiNi and $Ti_{0.98}Ni_{1.02}$ are also formed by the fast solidification of the melt. The intermetallic compounds and the amorphous phases and nanograins exhaust the ductility and increase the risk of brittle fracture of deformed metal. The bamboo-shaped cracks are formed in the melting zone.

3.4 Microstructural Formation of the Heat Affected Zone

The heat affected zone is one of the features of the explosive cladding technique. During the explosive cladding process, the stress as well as the deformation on the Ti tube is uniform and axisymmetric in theory (Fig. 9). Boundaries of the melting zone and the heat affected zone should be circular arcs, whose center points to the center of the NiCr bar. Due to the excess of the explosives, the jet washes out the cladding interface, and an irregular wave curve-shaped melting zone boundary is formed, as shown in Fig. 3(a) and (b).

Our pervious study indicated that the shear bands with fine equiaxed grains should formed in this zone on the Ti side in the Ti/mild steel explosive cladding plate's interface (Ref 6). However, the shear bands disappear in this work. According to the above results, the heat affected zone is characterized by bulky grains with low dislocation density and low microhardness. And the microtextures of the heat affected zone are also different from those of the region near to the heat affected zone in Ti tube. These results confirm that recrystallization should have occurred in the heat affected zone and fine grains experience significantly growth during the deformation process. How does it happen?

Author's personal copy

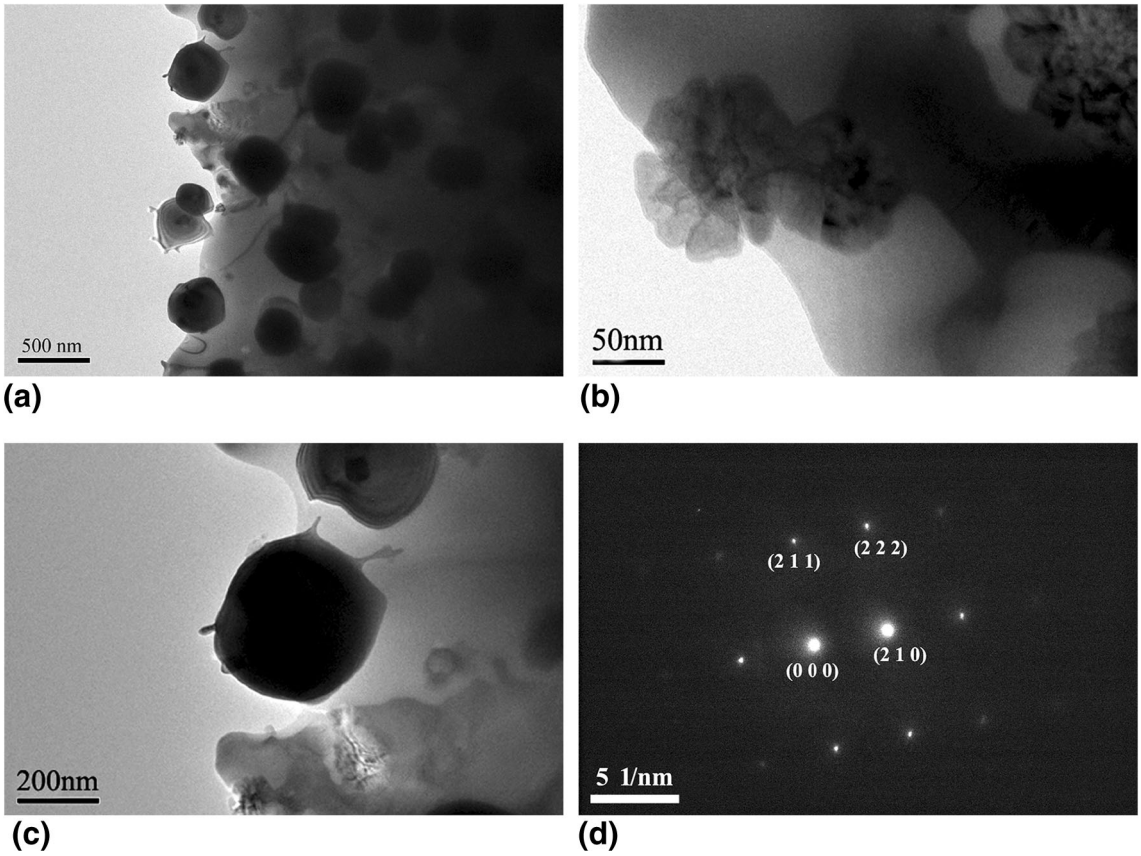

Fig. 4 Transmission electron micrographs of the melting zone, (a) micrographs of the melting zone, (b) transparent snowflake nanograins, (c) the scattered grains, and (d) the selected area diffraction pattern corresponding to (c)

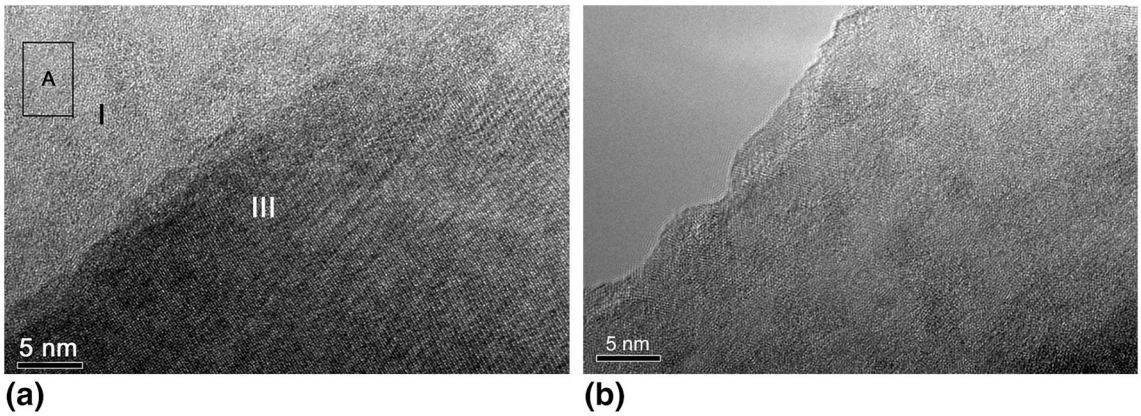

Fig. 5 (a, b) High-resolution crystal lattice images of selected area

The temperature field of the heat affected zone can be illustrated as follows (Ref 27):

$$T(x, t_{\mathrm{T}}) = \frac{(T_{\max} - T_0) \cdot \delta}{\sqrt{4 \cdot \pi \cdot k \cdot t_{\mathrm{T}}}} \cdot e^{-\frac{x^2}{4 \cdot k \cdot t_{\mathrm{T}}}}, \quad \text{(Eq 7)}$$

$$\delta = \frac{\delta_1}{2} + \delta_2, \quad \text{(Eq 8)}$$

where k is the thermal diffusion coefficient, x is the distance from the center point, and t_{T} is the time of thermal transmission, and $T_{\max}$ and T_0 are the maximum temperature and the room temperature; δ_1 and δ_2 are the average widths of the melting zone and the heat affected zone, respectively. The parameter t_{T} is defined as follows:

$$t_{\mathrm{T}} = \frac{x^2}{2 \cdot k}. \quad \text{(Eq 9)}$$

The melting points of pure Ti and NiCr alloy are 1941 K (1668 °C) and 1673 K (1400 °C), respectively. The temperature in the melting zone is higher than the melting point of both pure Ti and NiCr alloys for the reason that the intermetallics and amorphous phases are generated in the melting zone. The parameters used in Eq 7 are that T_0 is 298 K (25 °C), δ_1 is

Author's personal copy

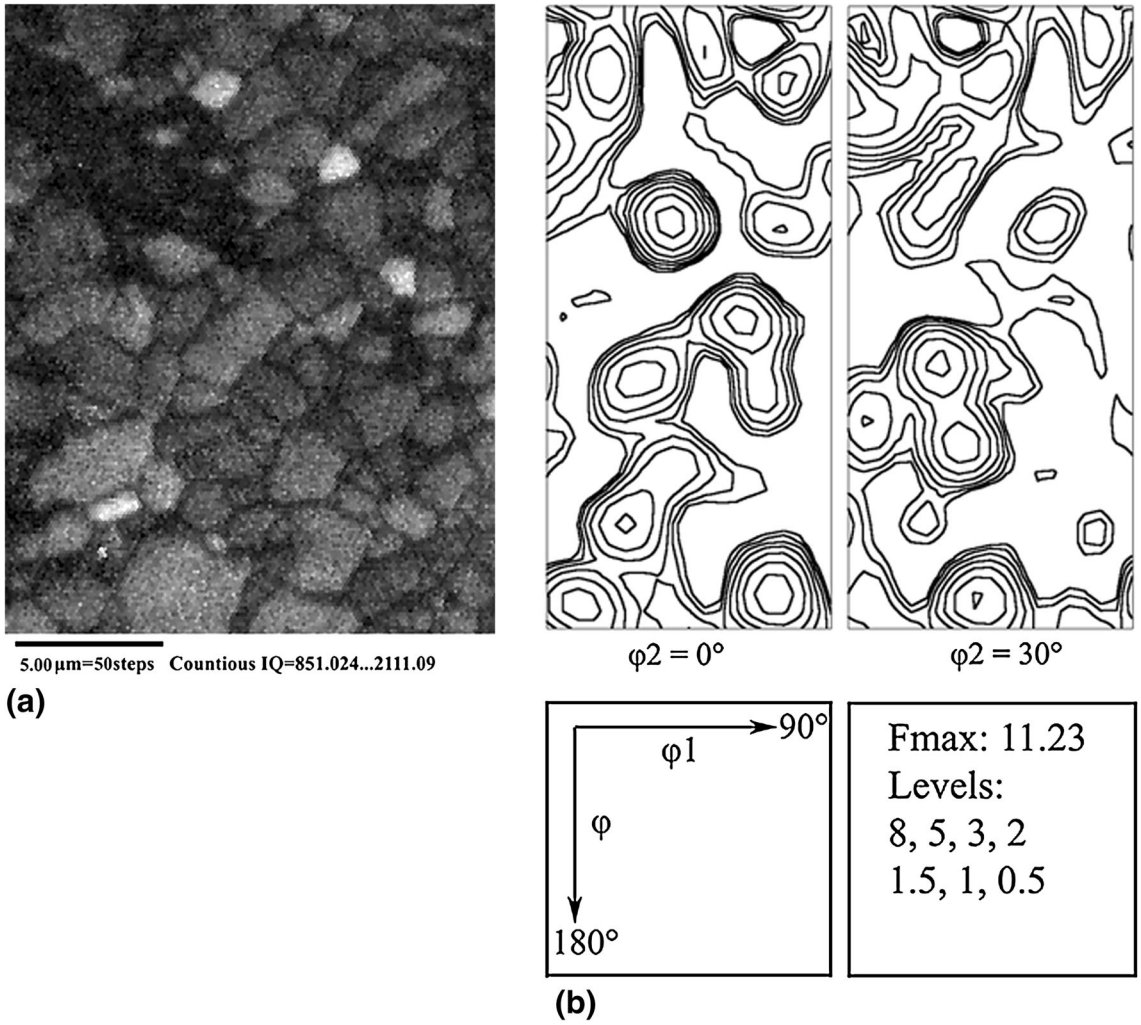

Fig. 6 (a) Image quality map shows grains in the region near the heat affected zone in CP-Ti tube and (b) corresponding orientation distribution function maps

80 µm, and δ_2 is 60 µm. Substituting Eq 9 into Eq 7, the temperature of the heat affected zone can be obtained as follows:

$$T = \frac{(T_{\max} - 298)}{\sqrt{2\pi}} \cdot \frac{1}{\sqrt{e}} \cdot \frac{0.0001}{x} \quad (x \geq 40\,\mu\text{m}). \qquad \text{(Eq 10)}$$

When x is 40 µm, T is about 1941 K (1668 °C) at least. So, $T_{\max}$ in the melting zone is 3507 K (3234 °C). Then,

$$T = \frac{0.077648}{x}. \qquad \text{(Eq 11)}$$

Combining Eq 11 with Eq 5, the temperature-distance and the temperature-time curves are demonstrated in the Fig. 10. It can be seen that the temperature fast declines with the distance and the time of thermal transmission increases when the distance from the interface x is larger than 40 µm. When the distance from the interface is more than 100 µm, the temperature is close to 776.4 K (503.4 °C) (about 0.4 T_m). Therefore, the temperature in the heat affected zone can meet with the needs for the recrystallization of pure Ti during the deformation process.

According to the conventional grain growth theory, a continuous grain growth can be illustrated as follows (Ref 28):

$$L^n - L_0^n = k(T) \cdot t, \qquad \text{(Eq 12)}$$

where L is the final mean grain size, L_0 is the initial grain size, n is the grain growth exponent, and k (T) is a temperature dependent constant. The parameter k (T) is defined as follows:

$$k(T) = k_0 \cdot \frac{1}{e^{\left(\frac{Q}{RT}\right)}}, \qquad \text{(Eq 13)}$$

where k_0 is the pre-exponential coefficient, R is the gas constant, and Q is the activation energy for grain growth. The maximum temperature (T) and possible deformation time (t) and possible initial grain size (L_0) in the heat affected zone are 1941 K (1668 °C) and 10 ms and 4 µm, respectively. For pure Ti, Q and R are 204 kJ/mol and 8.314 J/mol, k_0 and n are $1 \times 10^{4.2}$ and 0.5 (Ref 29), respectively. Then, the calculated $k(T)$ and L are 0.0513 and 4.002 µm, respectively. The calculated final grain size is much smaller than the observed one whose grain size L is about 60 µm shown in Fig. 3(d). What is more, the continuous grain growth model suggests that sizes of grains in the heat affected zone should be emerged as a gradient distribution of the distance from the melting zone. However, it is in contrast with that the experi-

Author's personal copy

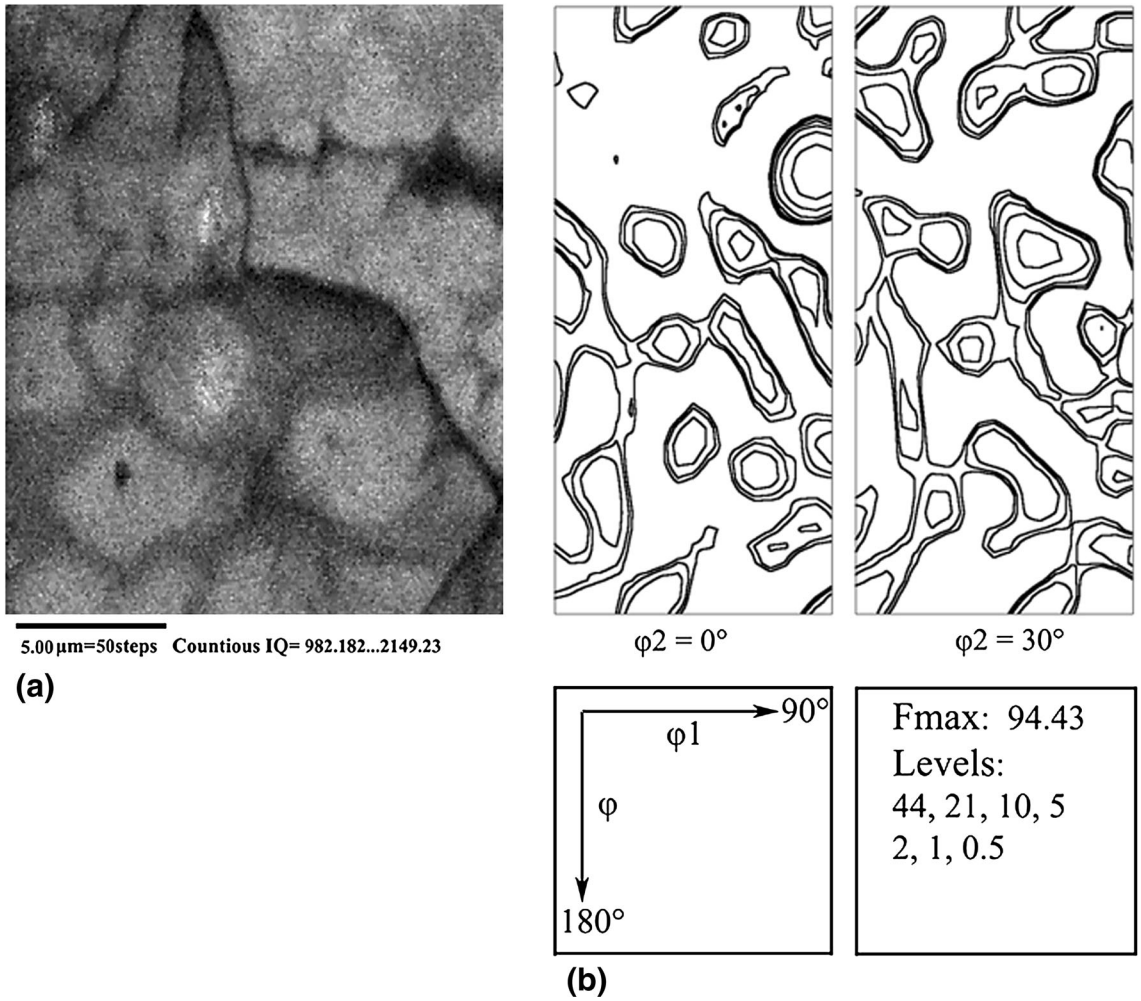

Fig. 7 (a) Image quality map shows grains in the heat affected zone and (b) corresponding orientation distribution function maps

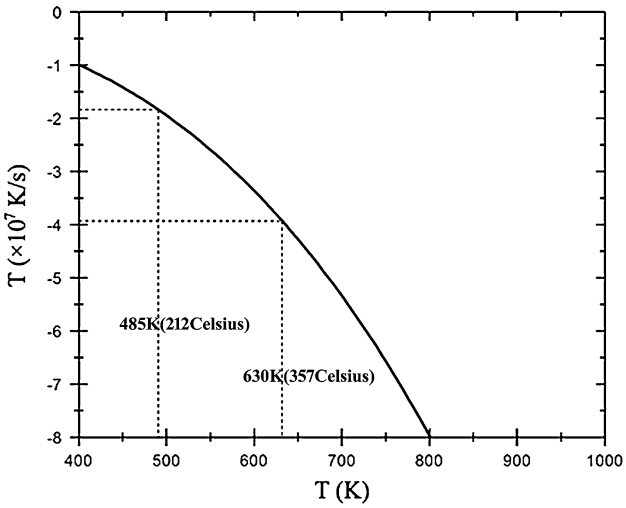

Fig. 8 The cooling rate (V) vs. temperature (T) curves obtained within the melting zone

mental results illustrate (Fig. 3b). The sizes of grains in the heat affected zone are relatively uniform, and they are change obviously at the edge of the heat affected zone marked by "B" (Fig. 3b). Therefore, the conventional grain growth theory cannot explain the grains growth within the heat affected zone, and these fine recrystallized grains in the heat affected zone should have undergone an abnormal growth during the deformation time.

Figure 3(d) shows that some of grain boundaries are disappeared partially at the locations marked by symbols "a1", "a2", "a3", etc., and some of grain boundaries are even disappeared completely at the places marked by symbols "A1" and "A2." The phenomena are also characterized in the 718 alloy after heating at a peak temperature of 1500 K (1227 °C) (Ref 30). It indicated that the rapid grain growth could be resulted from the sudden disappearance of some of the boundaries. Hence, the excessive grain growth in the heat affected zone can be explained by the sudden absence of some grain boundaries with assistant of severe deformation and high temperature. From the above analysis, the microstructural formation of the heat affected zone can be illustrated as follows: the dislocations accumulate to form elongated cell structures firstly, and then the cell structures break up to form subgrains, and then the subgrains rotate to form recrystallized grains, and finally recrystallized grains grow up to bulky grains in the way of the absence of grain boundaries.

Author's personal copy

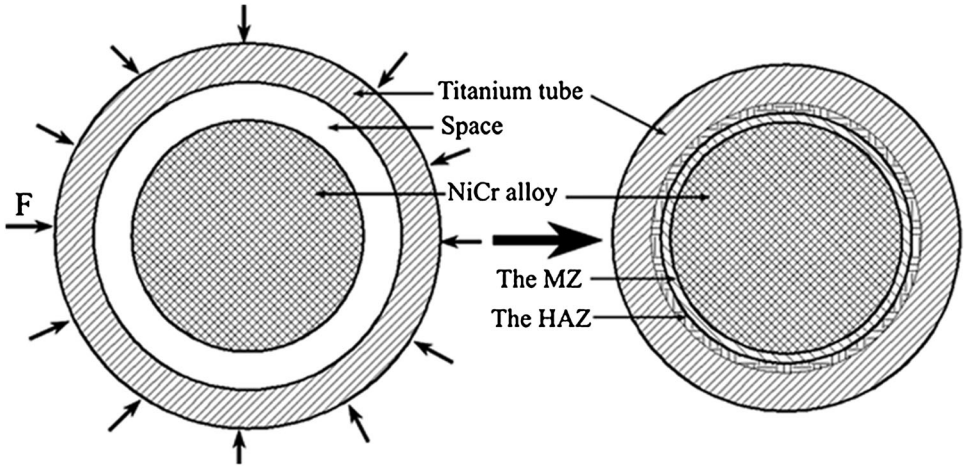

Fig. 9 Schematic of the deformation distribution on the Ti side

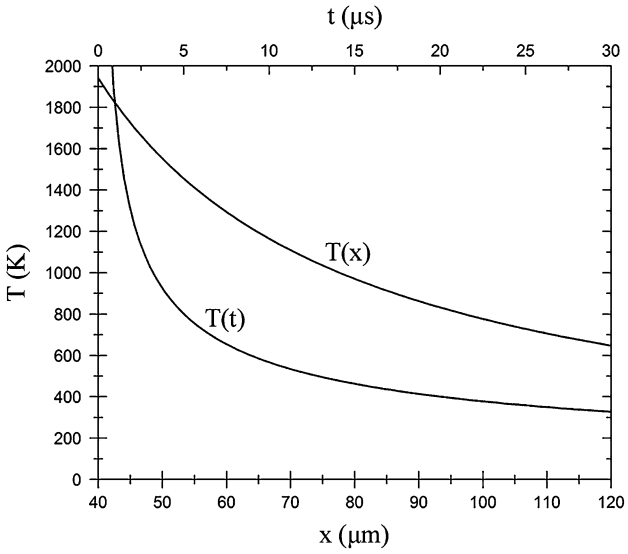

Fig. 10 The temperature vs. distance and time curves obtained within the heat affected zone

4. Conclusions

The Ti tube and the NiCr alloy bar were bonded successfully through explosive cladding process. The melting zone and the heat affected zone are generated at the cladding interface. The average bonding strength is 154.39 MPa.

The intermetallics, nanograins, and amorphous phases coexist in the melting zone. Quantitative analysis indicates that the cooling rate ranges from 1.78×10^7 to 3.89×10^7 K/s (1.78×10^7 to 3.89×10^7 °C/s) at the amorphous transition temperature. High cooling rate in the zone is the main reason for the formation of intermetallics, nanograins, and amorphous phases.

The heat affected zone consists of bulky grains with sizes about 60 μm and low dislocation density. The microtextures of the heat affected zone are different from those of the region near the heat affected zone in CP-Ti tube. Grains in the heat affected zone experience recrystallization and abnormal grain growth during the deformation process. The excessive grain growth can be explained by the absence of grain boundaries.

Acknowledgments

This work was financial supported by the Hunan Provincial Natural Science Foundation of China (No. 12JJ2028), by the Major Science and Technology Project of Hunan in China (No. 2010F51004), and by a scholarship from the China Scholarship Council (No. 201308430093).

References

1. A.A. Ezra, *Principles and Practice of Explosive Metal Working*, Industrial Newspapers Limited, London, 1973
2. F. Findik, Recent Developments in Explosive Welding, *Mater. Des.*, 2011, **32**, p 1081–1093
3. M. Acarer and B. Demir, An Investigation of Mechanical and Metallurgical Properties of Explosive Welded Aluminum-Dual Phase Steel, *Mater. Lett.*, 2008, **62**, p 4158–4160
4. C. Sudha, T.N. Prasanthi, P.V. Thomas, S. Saroja, and M. Vijayalakshmi, Metastable Phase Transformation in Ti-5Ta-2Nb Alloy and 304L Austenitic Stainless Steel Under Explosive Cladding Conditions, *Metall. Mater. Trans. A*, 2012, **43**, p 3596–3607
5. P. Tamilchelvan, K. Raghukandan, and S. Saravanan, Optimization of Process Parameters in Explosive Cladding of Titanium/Stainless Steel 304L Plates, *Int. J. Mater. Res.*, 2013, **104**, p 1205–1211
6. Y. Yang, B.F. Wang, J. Xiong, X.Y. Yang, Y. Zeng, and Z.P. Chen, Adiabatic Shear Bands on the Titanium Side in the Titanium/Mild Steel Explosive Cladding Interface: Experiments, Numerical Simulation, and Microstructure Evolution, *Metall. Mater. Trans. A*, 2006, **37**, p 3131–3137
7. P. Mallesham, A.A. Gokhale, and V.S.R. Murti, Nature of the Interface Between AA7072 Alloy Explosively Clad to AA8090 Aluminium Alloy, *J. Mater. Sci.*, 2012, **38**, p 1869–1873
8. M. Acarer, Electrical, Corrosion, and Mechanical Properties of Aluminum-Copper Joints Produced by Explosive Welding, *J. Mater. Eng. Perform.*, 2012, **21**, p 2375–2379
9. H. Paul, L. Lityńska-Dobrzyńska, and M. Prażmowski, Microstructure and Phase Constitution Near the Interface of Explosively Welded Aluminum/Copper Plates, *Metall. Mater. Trans. A*, 2013, **44**, p 3836–3851
10. H. Zhao, P.C. Li, Y.G. Zhou, Z.H. Huang, and H.N. Wang, Study on the Technology of Explosive Welding Incoloy800-SS304, *J. Mater. Eng. Perform.*, 2011, **20**, p 911–917

Author's personal copy

11. Y. Yang, B.F. Wang, and J. Xiong, Amorphous and Nanograins in the Bonding Zone of Explosive Cladding, *J. Mater. Sci.*, 2006, **41**, p 3501–3505
12. M. Honarpisheh, M. Asemabadi, and M. Sedighi, Investigation of Annealing Treatment on the Interfacial Properties of Explosive-Welded Al/Cu/Al Multilayer, *Mater. Des.*, 2012, **37**, p 122–127
13. B. Gulenc, Investigation of Interface Properties and Weldability of Aluminum and Copper Plates by Explosive Welding Method, *Mater. Des.*, 2008, **29**, p 275–278
14. J.L. Caron, S.S. Babu, and J.C. Lippold, Welding-Induced Microstructure Evolution of a Cu-Bearing High-Strength Blast-Resistant Steel, *Metall. Mater. Trans. A*, 2011, **42**, p 4015–4031
15. B. Wronka, Testing of Explosive Welding and Welded Joints. Wavy Character of the Process and Joint Quality, *Int. J. Impact Eng.*, 2011, **38**, p 309–313
16. I.A. Bataev, A.A. Bataev, V.I. Mali, and D.V. Pavliukova, Structural and Mechanical Properties of Metallic-Intermetallic Laminate Composites Produced by Explosive Welding and Annealing, *Mater. Des.*, 2012, **35**, p 225–234
17. J.E. Garay, U. Anselmi-Tamburini, and Z.A. Munir, Enhanced Growth of Intermetallic Phases in the Ni-Ti System by Current Effects, *Acta Mater.*, 2003, **51**, p 4487–4495
18. M.A. Meyers, Y.B. Xu, Q. Xue, M.T. Perez-Prado, and T.R. McNelley, Microstructural Evolution in Adiabatic Shear Localization in Stainless Steel, *Acta Mater.*, 2003, **51**, p 1307–1325
19. Y. Yang, F. Jiang, B.M. Zhou, X.M. Li, H.G. Zheng, and Q.M. Zhang, Microstructural Characterization and Evolution Mechanism of Adiabatic Shear Band in a Near Beta-Ti Alloy, *Mater. Sci. Eng. A*, 2011, **528**, p 2787–2794
20. L. Tang, Z. Chen, C. Zhan, X. Yang, and C. Liu, Microstructure and Microtexture Evolution of Shear Localization in Dynamic Deformation with Different Strains in Annealed Copper, *Metall. Mater. Trans. A*, 2013, **44**, p 793–805
21. Y.B. Xu, W.L. Zhong, Y.J. Chen, L.T. Shen, Q. Liu, Y.L. Bai, and M.A. Meyers, Shear Localization and Recrystallization in Dynamic Deformation of 8090 Al-Li Alloy, *Mater. Sci. Eng. A*, 2001, **299**, p 287–295
22. B.F. Wang, W. Chen, J. Li, Z.L. Liu, and X.B. Zhu, Microstructure and Formation of Melting Zone in the Interface of Ti/NiCr Explosive Cladding Bar, *Mater. Des.*, 2013, **47**, p 74–79
23. O. Dezellus, M. Zhe, F. Bosselet, D. Rouby, and J. Viala, Mechanical Testing of Titanium/Aluminium-Silicon Interface. Effect of T6 Heat Treatment, *Mater. Sci. Eng. A*, 2011, **528**, p 2795–2803
24. J. Tarasiuk, Ph. Gerber, and B. Bacroix, Estimation of Recrystallized Volume Fraction from EBSD Data, *Acta Mater.*, 2002, **50**, p 1467–1477
25. S. Wronski, J. Tarasiuk, B. Bacroix, K. Wierzbanowsk, and H. Paul, Microstructure Heterogeneity After the ECAP Process and Its Influence on Recrystallization in Aluminium, *Mater. Charact.*, 2013, **78**, p 60–68
26. H.H. Yan and X.J. Li, Theoretical Explanation for Amorphous Phase Emerging Across the Interface During Explosive Welding, *Rare. Met. Mater. Eng.*, 2003, **32**, p 176–182
27. Y. Yang, Z.H. Li, and P.C. Lu, A Temperature Distribution Model of Explosive Cladding Interface and Its Application, *Rare. Met. Mater. Eng.*, 2000, **29**, p 161–163
28. S.S. Sahay, C.P. Malhotra, and A.M. Kolkhede, Accelerated Grain Growth Behavior During Cyclic Annealing, *Acta Mater.*, 2003, **51**, p 339–346
29. F.X. Gil, D. Rodriguez, and J.A. Planell, Grain Growth Kinetics of Pure Titanium, *Scripta Metall. Mater.*, 1995, **33**, p 1361–1366
30. B. Radhakrishnan and R.G. Thompson, Kinetics of Grain Growth in the Weld Heat Affected Zone of Alloy 718, *Metall. Mater. Trans. A*, 1993, **24**, p 2773–2785